Supplemental Information for

The Smallest 4f-Metalla-Aromatic Molecule of Cyclo-PrB$_2^-$ with Pr–B Multiple Bonds

Zhen-Ling Wang[1+], Teng-Teng Chen[2+], Wei-Jia Chen[2], Wan-Lu Li[1], Jing Zhao[1], Xue-Lian Jiang[3], Jun Li[1,3], Lai-Sheng Wang[2]* and Han-Shi Hu[1]*

[1]Department of Chemistry and Key Laboratory of Organic Optoelectronics & Molecular Engineering of Ministry of Education, Tsinghua University, Beijing 100084, China

[2]Department of Chemistry, Brown University, Providence, Rhode Island 02912, USA.

[3]Department of Chemistry, Southern University of Science and Technology, Shenzhen 518055, China

[+]These authors contributed equally to this work.

*E-mail: Lai-Sheng_Wang@brown.edu; hshu@mail.tsinghua.edu.cn

Table S1. Computational relative energies of the optimized PrB_2^- anion based on different initial structures ($C_{\infty v}$, C_{2v}, and C_s) and spin multiplicities ($2S+1$).[a] The calculations were done at the level of PBE0/TZP using ADF code.

	Singlet	Triplet	Quintet	Septet
$C_{\infty v}$	112.75	45.47	50.93	81.80
C_{2v}	33.73	0	26.13	*[d]
C_s	32.66[b]	0.68[b]	24.05[c]	*[d]

[a] The initial structure of C_s has a 135-degree $\angle$Pr-B-B bond angle. Energies are given in kcal/mol and are relative to the lowest value (C_{2v} triplet, -498.68 kcal/mol). [b] The optimized structure is of C_{2v} symmetry. [c] The optimized structure is close to C_{2v} symmetry. [d] Not converged.

Note on the ground state of neutral PrB_2: As shown in Figure 2 and Table S1, PrB_2^- anion has a cyclo C_{2v} triangular geometry with a triplet $^3B_2$ ground state, which has an Kohn-Sham electron configuration $(4a_1)^2(3b_2)^2(2b_1)^2[(5a_1\alpha)^1(4b_2\alpha)^1](5a_1\beta)^1(6a_1\alpha)^1(7a_1\alpha)^1(6a_1\beta)^1$, where $(5a_1\alpha)^1(4b_2\alpha)^1$ corresponds to the quasi-atomic Pr f^2 configuration and $(\ldots)^2$ represent a pair of electrons on less spin-polarized orbitals. After comparing the energies of different electron occupation at PBE0/TZP level, we have determined that the neutral PrB_2 also has a C_{2v} geometry with quartet $^4B_2$ ground state of $(4a_1)^2(3b_2)^2(2b_1)^2$ $[(5a_1\alpha)^1(4b_2\alpha)^1](6a_1\alpha)^1(5a_1\beta)^1(7a_1\alpha)^1$ electron configuration. The calculated energy of this $^4B_2$ state of the neutral molecule is -463.11 kcal/mol, while the optimized $^2B_2$ doublet state of $(4a_1)^2(3b_2)^2(2b_1)^2$ $[(5a_1\alpha)^0(4b_2\alpha)^1](5a_1\beta)^1(6a_1\alpha)^1(7a_1\alpha)^1(6a_1\beta)^1$ electron configuration lies at -448.52 kcal/mol. A gap of about 15 kcal/mol is sufficient to demonstrate that the ground state of PrB_2 is the $^4B_2$ quartet.
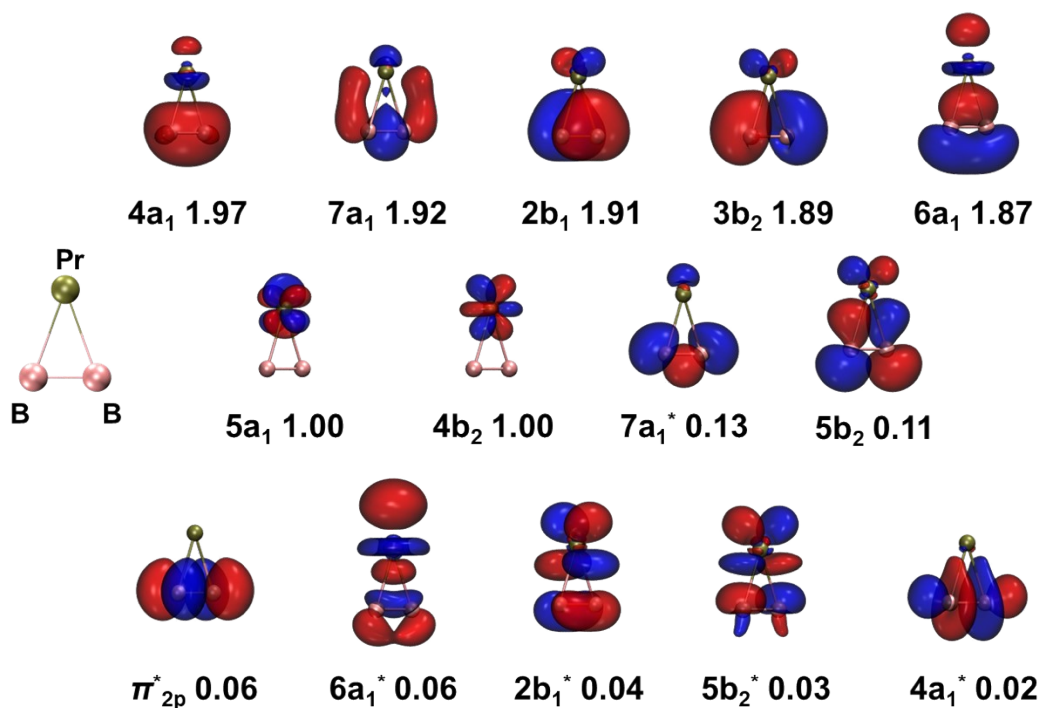
Figure S1. The CASSCF-(12e,14o) natural orbitals of the $^3B_2$ ground state of triangle PrB_2^- ion and their natural orbital occupation numbers (NOONs) calculated with MOLPRO code. Isovalue = 0.05 for all orbitals; colour codes for atoms: olive, Pr; pink, B. The orbitals are labelled to match the α set of K-S MOs if possible.

Selection of the active space: From Figure 4, one can see that Pr(III) has five significant bonding interactions with B_2^{4-} (MOs = $4a_1$, $3b_2$, $2b_1$, $6a_1$, and $7a_1\alpha + 5a_1\beta$) and two non-bonding 4f orbitals (MOs = $5a_1\alpha$ and $4b_2\alpha$), so six Pr related MOs were included in the active space. On the other hand, B_2^{4-} has eight valence MOs, and thus our CASSCF calculation has a total of 12 electrons in 14 MOs, denoted as CASSCF-(12e,14o). From the calculated results, $7a_1^*$, $5b_2$, π^*_{2p} natural orbitals having slightly larger NOONs correspond to B-B σ^*_{2p} and π^*_{2p} orbitals. The NOONs of other natural orbitals are close to integers and the first configuration dominates in the CI vector, indicating that the single-configurational methods like DFT and CCSD(T) would not have extremely large error for describing the bonding between Pr and B_2 moiety of these systems.

Table S2(a). The CASSCF-(12e,14o) CI vectors of C_{2v} *triangle* PrB$_2^-$ *ion*. The order of the labels of orbitals follows Figure S1.[a]

4a$_1$	2b$_1$	3b$_2$	7a$_1$	5a$_1$	4b$_2$	6a$_1$	7a$_1^*$	5b$_2$	π^*_{2p}	2b$_1^*$	6a$_1^*$	5b$_2^*$	4a$_1^*$	Coeff.
							Occupation Numbers							
2	2	2	2	2	1	1								0.892
2	2	2	2		1	1		2						-0.131
2		2	2	2	1	1	2							-0.112
2	2	2		2	1	1	2							-0.100
2	2		2	2	1	1			2					-0.081
2	2	2	2		1	1				2				-0.069
2	2	2		2	1	1		2						-0.067
2	2		2	2	1	1						2		-0.064
						$\vdots$								$\vdots$

Table S2(b). The Mulliken contributions (%) of each CASSCF-(12e,14o) natural orbital of C_{2v} *triangle* PrB$_2^-$ *ion*. The order of the labels of orbitals follows Figure S1.[a]

Atom	Mulliken Contribution (%)						
	4a$_1$	2b$_1$	3b$_2$	7a$_1$	5a$_1$	4b$_2$	6a$_1$
Pr	30.9	62.3	28.6	26.0	25.8	100.0	99.4
B	34.6	18.8	35.7	37.0	37.1	0.0	0.3
B	34.6	18.8	35.7	37.0	37.1	0.0	0.3
	7a$_1^*$	5b$_2$	π^*_{2p}	2b$_1^*$	6a$_1^*$	5b$_2^*$	4a$_1^*$
Pr	36.3	22.2	3.2	64.2	58.1	41.6	5.9
B	31.8	38.9	48.4	17.9	20.9	29.2	47.1
B	31.8	38.9	48.4	17.9	20.9	29.2	47.1

[a] The natural orbitals (Fig. S1) from the CASSCF-(12e,14o) first-order reduced density matrix are consistent with the Kohn-Sham MOs characters as schematically shown in Fig. 4: NOs 4a$_1$, 3b$_2$ $\leftrightarrow$ 1σ, 2σ; 2b$_1$, 5a$_1$ $\leftrightarrow$ $\pi_\perp$ $\pi_\parallel$; 7a$_1$ $\leftrightarrow$ 3σ; 5a$_1$, 4b$_2$ $\leftrightarrow$ Pr(III) f^2; 7a$_1^*$, 5b$_2$, π^*_{2p} $\leftrightarrow$ B-B σ^*_{2p} and π^*_{2p}.
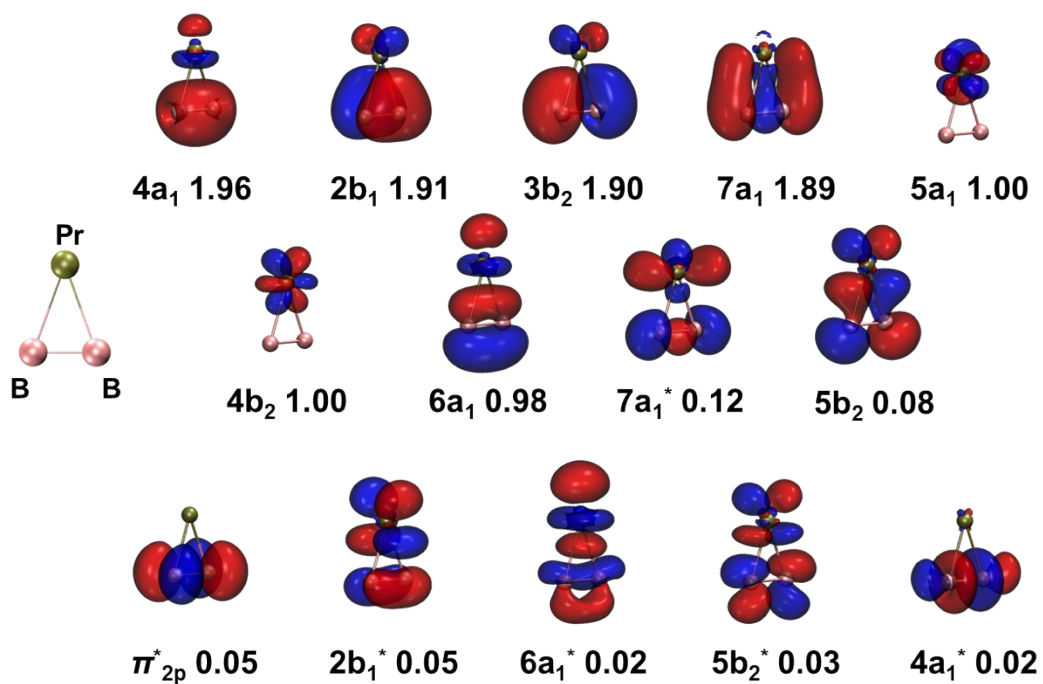
Figure S2. The CASSCF-(11e,14o) natural orbitals of the $^4B_2$ ground state of triangle PrB_2 neutral molecule and their natural orbital occupation numbers (NOONs). Isovalue = 0.05 for all orbitals; colour codes for atoms: olive, Pr; pink, B. The orbitals are labelled to match the α set of Kohn-Sham MOs if possible.

Table S3. The CASSCF-(11e,14o) CI vectors of C_{2v} *triangle* PrB$_2$ *neutral molecule*. The order of the labels of orbitals follows Figure S2.

Occupation Numbers														Coeff.
$4a_1$	$2b_1$	$3b_2$	$7a_1$	$5a_1$	$4b_2$	$6a_1$	$7a_1^*$	$5b_2$	π_{2p}^*	$2b_1^*$	$6a_1^*$	$5b_2^*$	$4a_1^*$	
2	2	2	2	1	1	1								0.906
2	2	2		1	1	1	2							-0.138
2	2		2	1	1	1		2						-0.082
2		2	2	1	1	1			2					-0.082
2		2	2	1	1	1				2				-0.075
						$\vdots$								$\vdots$

Table S4. Significant (>5%) fragment orbital contributions (Mulliken, in %) in Kohn-Sham MOs of *triangle* PrB$_2^-$. The MOs were calculated with PBE0/TZP using ADF code and are listed in decreasing order of energy.

	Orbital Energy	B$_2^-$				Pr			
$^3B_2$ C_{2v} PrB$_2^-$									
α-Set	(eV)	σ_{2s}	σ_{2s}^*	π_{2p}	σ_{2p}	6s	4f	5d	6p
$7a_1$ (HOMO)	-1.78			15	15	50	8	6	
$6a_1$ (HOMO-1)	-1.90			38	22			19	9
$4b_2$ (SOMO)	-2.26						91	5	
$5a_1$ (SOMO-1)	-2.33			5			86		
$2b_1$ (HOMO-2)	-2.46			62				34	
$3b_2$ (HOMO-3)	-3.95		62				6	26	
$4a_1$ (HOMO-4)	-9.26	83						8	
β-Set		σ_{2s}	σ_{2s}^*	π_{2p}	σ_{2p}	6s	4f	5d	6p
$6a_1$ (HOMO)	-1.77			57		25			8
$5a_1$ (HOMO-1)	-1.97			6	51	20		12	
$2b_1$ (HOMO-2)	-2.43			67				30	
$3b_2$ (HOMO-3)	-4.00		73					21	
$4a_1$ (HOMO-4)	-9.35	84						8	
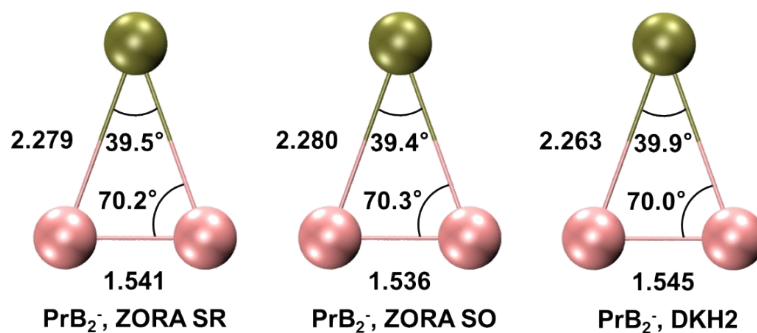
Figure S3. The global-minimum structures of PrB_2^- calculated with PBE0/TZP considering scalar ZORA relativistic effect (SR) or also with ZORA noncollinear spin-orbit coupling (SO), using the ADF code, and the global-minimum structure calculated with DKH2 Hamiltonian, PBE0 functional, SARC-DKH2 basis set for Pr, and cc-pVTZ basis set for B, using the Gaussian 16 code. The bond lengths are given in Å and the bond angles are given in degree (º). Colour codes: olive – Pr; pink – B.

Implication of SO calculations

Comparing Figure S7 and Figure 1, and Table S8 and Table 2, one can see that the change in geometry and electronic structure when including SO coupling is minimal, indicating that the spin-orbit coupling effect for the geometry and ground-state properties of this molecule is not significant.

Table S5. Cartesian coordinates for optimized PrB_2^- and PrB_2 with PBE0 functional.

TZP basis set at scalar relativistic (SR) level

PrB_2^-

Pr	0.000000	0.000000	0.279631
B	0.000000	0.770728	-1.864966
B	0.000000	-0.770728	-1.864966

Centre of current at 1.5 a_0 above the ring (Figure 6(b))

	0.000000	0.000000	-1.4522

PrB_2

Pr	0.000000	0.000000	0.311067
B	0.000000	0.763717	-1.880684
B	0.000000	-0.763717	-1.880684

TZP basis set at spin-orbit coupling (SO) level

PrB_2^-
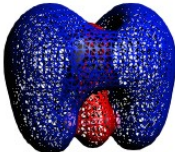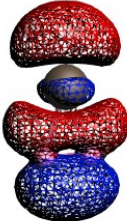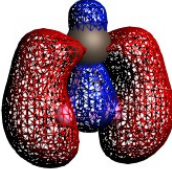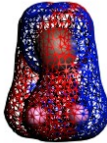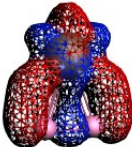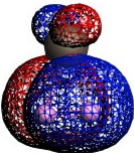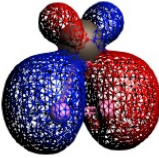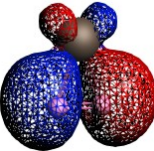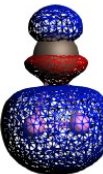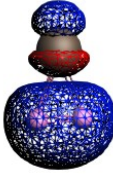
Pr	0.000000	-0.000007	0.281301
B	0.000000	0.767877	-1.865810
B	0.000000	-0.767868	-1.865789

cc-pVTZ basis set for B and SARC-DKH2 basis set for Pr

PrB_2^-

Pr	0.000000	0.000000	-0.308205
B	0.000000	0.772463	1.818407
B	0.000000	-0.772463	1.818414

Table S6. The Kohn-Sham spinors of PrB_2^- calculated with PBE0/TZP and noncollinear spin-orbit coupling effect at the global minimum structure using ADF code. Isovalue = 0.03; colour code for atoms: olive – Pr; pink – B.

kind	$-\varepsilon_i$ (eV)	contour	kind	$-\varepsilon_i$ (eV)	contour
3σ	1.72		$\pi_\parallel$	1.79	
$\pi_\parallel$	1.93		3σ	1.99	
f^2	2.26		f^2	2.34	
$\pi_\perp$	2.47		$\pi_\perp$	2.59	
2σ	3.87		2σ	4.04	
1σ	9.27		1σ	9.39	

Figure S4. The Kohn-Sham canonical MO energy levels of linear PrB_2^-, B_2^-, and Pr calculated with PBE0/TZP using ADF code. The energy levels of PrB_2^- are shifted to match the 4f levels in Pr and PrB_2^-, and the energy levels of B_2^- are shifted to match the 1s levels in C_{2v} PrB_2^- and B_2^-. Singly occupied 4f MO levels are 1δ.
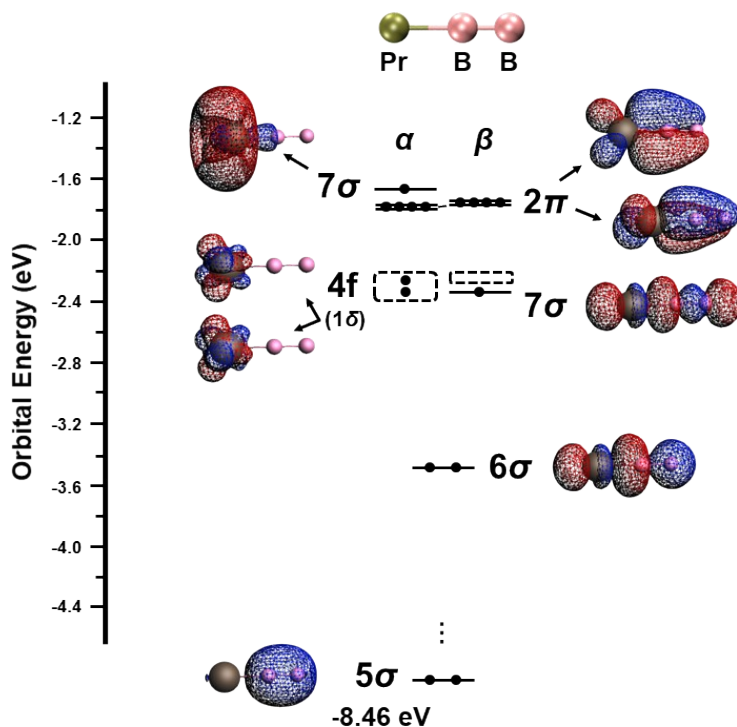
Figure S5. The Kohn-Sham canonical MOs of $C_{\infty v}$ *linear* PrB_2^- calculated with PBE0/TZP using ADF code. The energy levels of PrB_2^- are shifted to match the 4f levels in Pr and PrB_2^-. Isovalue = 0.03 for all orbitals; colour codes for atoms: olive – Pr; pink – B.

Table S7. Significant (>5%) fragment orbital contributions (Mulliken, in %) in Kohn-Sham MOs of *linear* PrB_2^-. Orbitals are listed in decreasing order of energy calculated with PBE0/TZP using ADF code.

$^3\Gamma\ C_{\infty v}\ PrB_2^-$									
	Orbital Energy	B_2^-				Pr			
α-Set	(eV)	σ_{2s}	σ^*_{2s}	π_{2p}	σ_{2p}	6s	4f	5d	6p
7σ (HOMO)	-1.68				5	56		18	13
2π (HOMO-1)	-1.76			40				55	
1δ (SOMO)	-2.30						94	5	
6σ (HOMO-2)	-3.47		48			13		18	
5σ (HOMO-3)	-8.46	93							
β-Set		σ_{2s}	σ^*_{2s}	π_{2p}	σ_{2p}	6s	4f	5d	6p
2π (HOMO-1)	-1.75			89				10	
7σ (HOMO)	-2.37				53	19		21	
6σ (HOMO-2)	-4.44		79		9			6	
5σ (HOMO-3)	-9.92	95							

Table S8(a). $NICS_{zz}(\zeta)$ values of PrB_2^-, B_3^-, and $C_3H_3^+$ computed at the centre of the ring current (for PrB_2^-, the centre is shown in Figure 6(b)) with PBE0 functional, MWB28 ECP and basis set for Pr, and cc-pVTZ basis set for light elements, using Gaussian 16.

	$C_3H_3^+$	B_3^-	PrB_2^-
$\zeta = 0$	-33.0	-76.7	-284.6
$\zeta = 0.2$	-35.1	-74.4	-269.4
$\zeta = 0.4$	-38.2	-67.8	-228.1
$\zeta = 0.6$	-38.3	-58.6	-172.0
$\zeta = 0.8$	-34.8	-48.9	-113.7
$\zeta = 1.0$	-29.5	-39.9	-62.5

Table S8(b). $NICS_{zz}(\zeta)$ values of PrB_2^-, B_3^-, and $C_3H_3^+$ computed at the centre of the ring current (for PrB_2^-, the centre is shown in Figure 6(b)) by ADF with PBE0/TZP all-electron basis, including the noncollinear spin-orbit coupling effect.

	$C_3H_3^+$	B_3^-	PrB_2^-
$\zeta = 0$	-32.3	-76.5	-242.2
$\zeta = 0.2$	-34.2	-74.2	-226.8
$\zeta = 0.4$	-37.0	-67.7	-190.9
$\zeta = 0.6$	-37.1	-58.7	-151.9
$\zeta = 0.8$	-33.8	-49.0	-118.3
$\zeta = 1.0$	-28.8	-40.1	-89.8

Table S9(a). NICS$_{zz}(\zeta)$ values of PrB$_2^-$ calculated by PBE0, BHandHLYP, and B3LYP using the Gaussian 16 program with MWB28 ECP and basis set for Pr and cc-pVTZ basis set for B. The centre of the ring current in Figure 6(b) (coordinates in Table S5 is chosen to be the centre point for these calculations.

PrB$_2^-$ NICS	PBE0	BHandHLYP	B3LYP
$\zeta = 0$	-284.6	-361.5	-227.6
$\zeta = 0.2$	-269.4	-342.0	-215.3
$\zeta = 0.4$	-228.1	-289.0	-182.0
$\zeta = 0.6$	-172.0	-216.8	-137.1
$\zeta = 0.8$	-113.7	-141.6	-90.7
$\zeta = 1.0$	-62.5	-75.5	-50.2

Table S9(b). The integrated ring current of PrB$_2^-$ on its B-B bond and Pr-B bond calculated by PBE0, BHandHLYP, and B3LYP using the Gaussian 16 program with MWB28 ECP and basis set for Pr and cc-pVTZ basis set for B. A positive ring-current value indicates the presence of a diamagnetic induced current. The centre of the ring current in Figure 6(b) (coordinates in Table S5) is chosen to be the centre point for these calculations.

PrB$_2^-$ Integrated Ring Current	PBE0	BHandHLYP	B3LYP
Along B-B Bond	7.2	6.7	6.9
Along Pr-B Bond	6.3	5.9	6.1
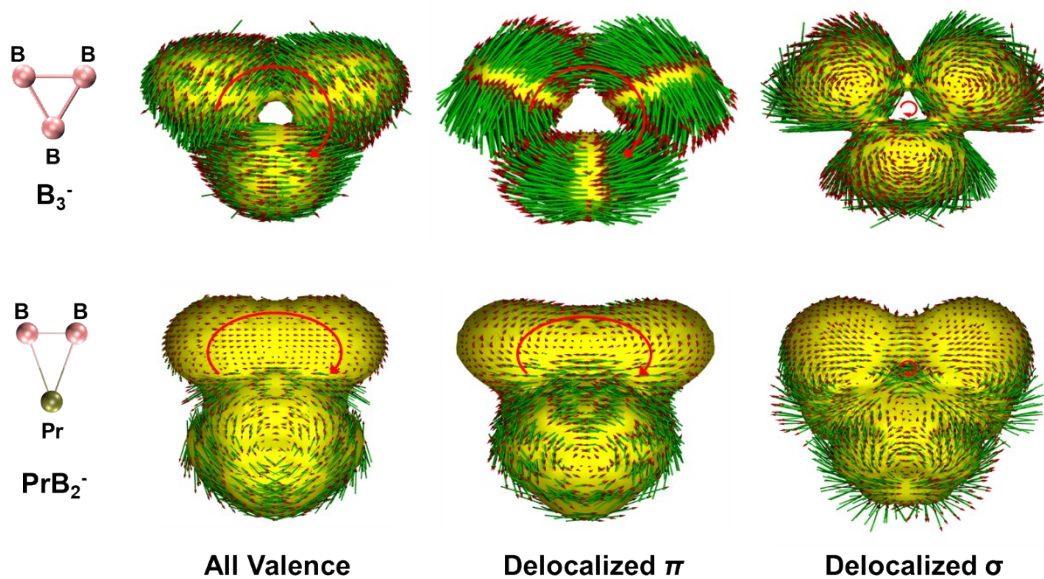
Figure S6. Isosurfaces of AICD (isovalue = 0.03) for PrB_2^- and B_3^- generated from all valence electrons, the delocalized π MO, and the delocalized σ MO, calculated by AICD and Gaussian 16 code with MWB28 ECP and basis set for Pr and cc-pVTZ basis set for B. Green arrows on the surfaces show the strength and the direction of the current induced by the magnetic field, which is pointing out of the molecule plane. The clockwise current represented by red arrows is diatropic and indicates aromaticity.
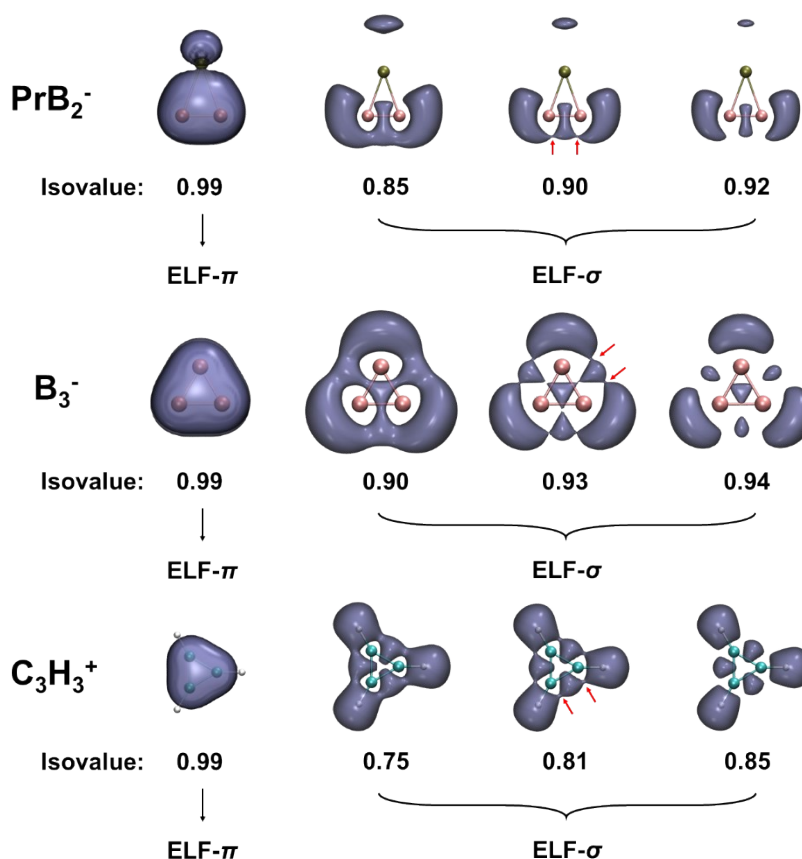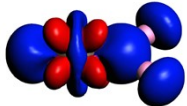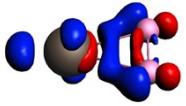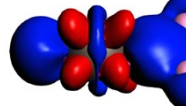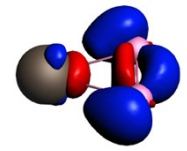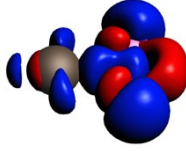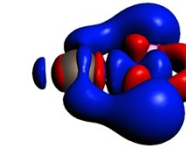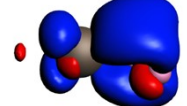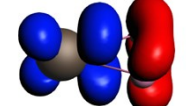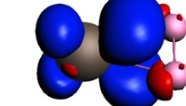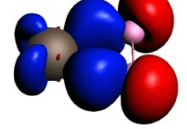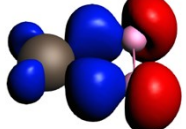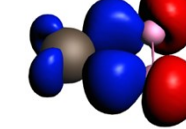
Figure S7. Results of bifurcation analysis of ELF-σ and ELF-π on PrB_2^-, B_3^- and $C_3H_3^+$ by using Gaussian 16 program. Some of the critical points are pointed out by red arrows; ELFs-π do not have any reasonable critical points. Colour codes for atoms: olive – Pr; pink – B; cyan – C; white – H.

Implication of bifurcation analysis of ELF

The process of bifurcation analysis is to increase the isovalue of the isosurface of ELF to see when it breaks into several disconnected parts. The higher the isovalue of the breaking critical point is, the stronger the delocalization of the electrons would be. ELF-π of all these systems do not break until isovalue reaches 0.99999, showing strong π-aromaticity. In σ systems, the critical point of PrB_2^- is closer to the known σ-aromatic B_3^-, providing evidence that PrB_2^- also possesses σ-aromaticity.

Table S10. Energy decomposition analysis of PrB_2^- and the associated deformation densities $\Delta\rho$ of the most important pairwise orbital interactions ΔE_{orb} (Isovalue = 0.002 au for α, β; Isovalue = 0.004 au for $\alpha+\beta$, unless specified). The direction of the charge flow is red to blue. The calculations were carried out at the level of PBE0/TZP using ADF code. Energy values are given in kcal mol^{-1}. Colour codes for atoms: olive – Pr; pink – B.

Fragments	Pr: s^2f^3		B_2^-: $^2\Pi_u$
ΔE_{Pauli}	381.11		
ΔE_{elstat}	-280.19		
ΔE_{orb}	-278.17		
	α	β	$\alpha+\beta$
$\Delta E_{orb}(\sigma)$			
	-89.63	-9.54	-99.17 (35.65 %)[a]
$\Delta E_{orb}(\sigma)$			
	-6.30	-48.68	-54.98 (19.76 %)
$\Delta E_{orb}(\pi)$			
	-45.40	-14.55	-59.95 (21.55 %)
$\Delta E_{orb}(\sigma)$			
	-20.15	-15.77	-35.92 (12.91 %)
$E_{bonding}$	-177.25		

[a] The value in parentheses gives the percentage contribution to the total orbital interactions ΔE_{orb}.
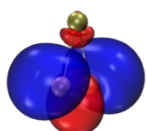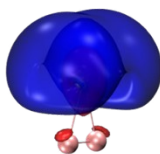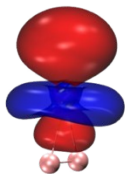
(a) Spin α

ON: 0.5985   ON: 0.3705   ON: 0.2822   ON: 0.2199

ON: 0.4014   ON: 0.6295   ON: 0.7178   ON: 0.7801
1st PIO   2nd PIO   3rd PIO   4th PIO
PBI: 0.2403   PBI: 0.2322   PBI: 0.2026   PBI: 0.1715
%: 28.08   %: 27.25   %: 23.67   %: 24.04

Spin β
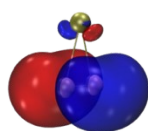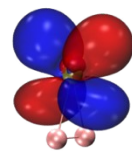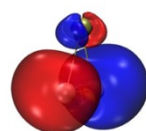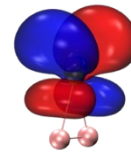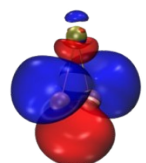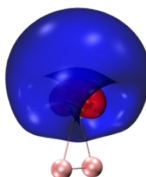
ON: 0.6119   ON: 0.2780   ON: 0.2279   ON: 0.1642

ON: 0.3881   ON: 0.6295   ON: 0.7721   ON: 0.8358
1st PIO   2nd PIO   3rd PIO   4th PIO
PBI: 0.2374   PBI: 0.2007   PBI: 0.1760   PBI: 0.1372
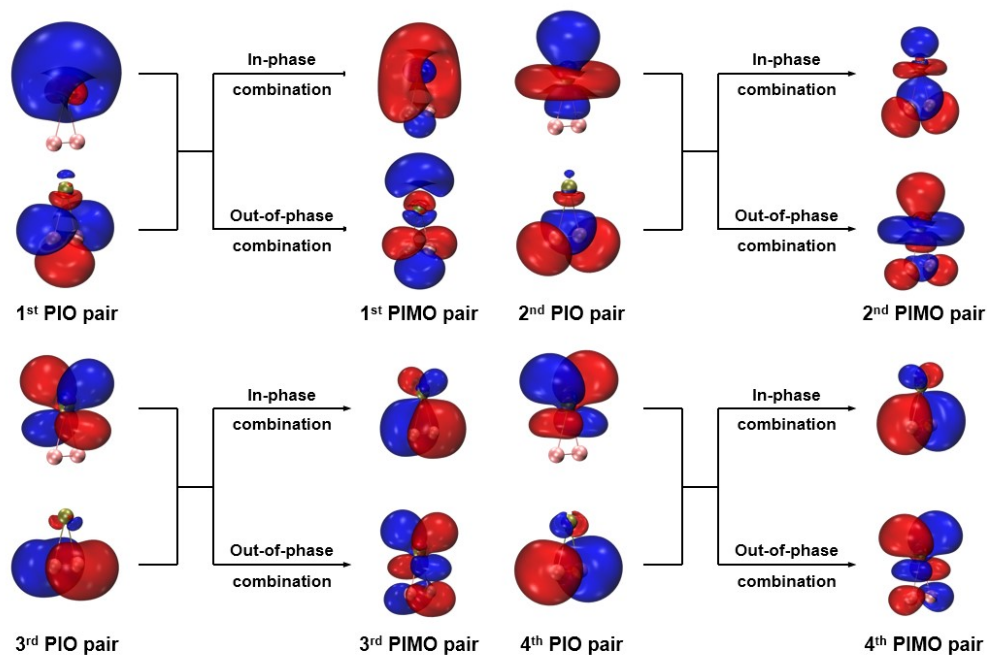%: 31.47   %: 26.60   %: 23.32   %: 18.18
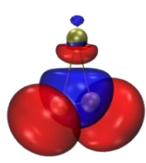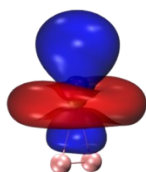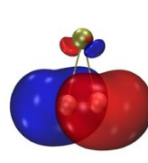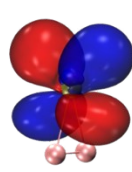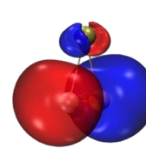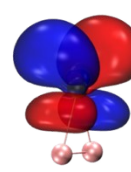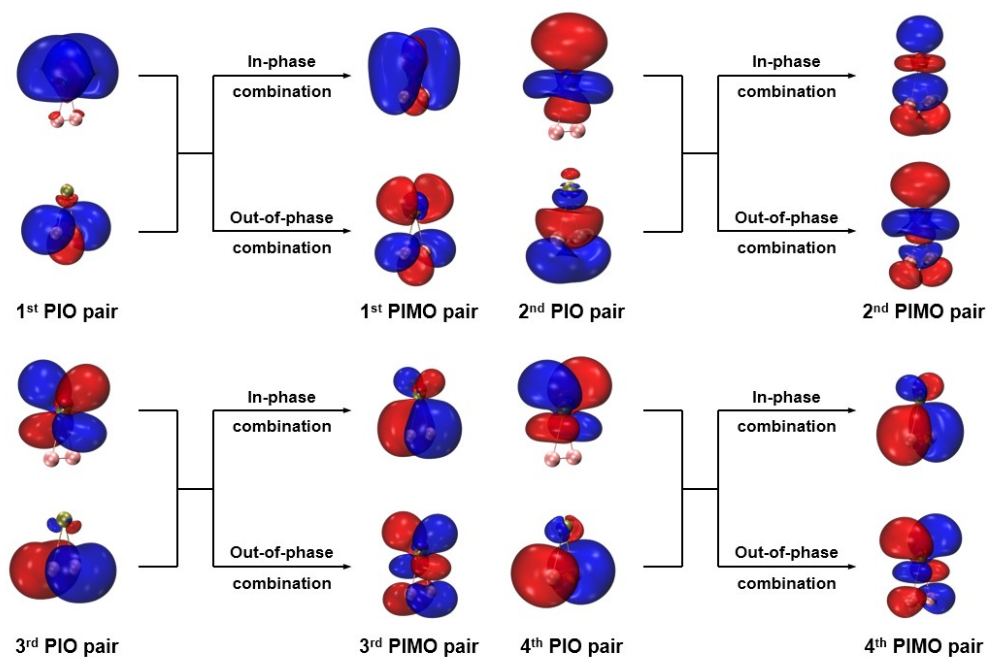
Figure S8. Results of PIO analysis by using Gaussian 16 program on PrB$_2^-$ with Pr and B$_2$ as two fragments. (a) Top four PIOs of each fragment. The occupation numbers are given as ON near each PIO pair, and the PIO-based bond indices (PBI) and its percentage contribution to the total interactions between two fragments are shown below each pair. (b) Top four PIMO pairs. Note that the phase of each PIO is naturally paired up with its counterpart. Isovalue = 0.03 for all orbitals; colour codes: olive – Pr; pink –B.